Original article

CoMFA and docking studies on triazolopyridine oxazole derivatives as p38 MAP kinase inhibitors

M. Ravi Shashi Nayana [a], Y. Nataraja Sekhar [a], N. Siva Kumari [a],
S.K. Mahmood [a,*], Muttineni Ravikumar [b]

[a] *Bioinformatics Division, Environmental Microbiology Lab, Department of Botany, Osmania University,
Hyderabad 500 007, A.P., India*
[b] *Biocampus, S-1, Phase-1, Technocrats Industrial Estate, Balanagar, Hyderabad 500 037, A.P., India*

Abstract

With the objective to design new chemical entities with enhanced inhibitory potencies against p38 MAP alpha kinase, the 3D-QSAR and Comparative Molecular Field Analysis (CoMFA) studies were carried out on triazolopyridine oxazole compounds as inhibitors of these kinase is presented here. The developed model gave q^2 value of 0.707 and r^2 value of 0.942 for CoMFA. The high leave-one-out (LOO) cross-validated correlation coefficient q^2 reveals that the model is a useful tool for the prediction of test set of 19 compounds that were not included in the training set of 55 compounds. The results not only lead to better understanding of structural requirements of p38 alpha inhibitors but also can help in the design of new potent inhibitors. The binding mode of the compounds at the active site of p38 MAP alpha kinase was explored using Glide docking program and hydrogen-bonding interactions were observed between the inhibitors and the target. The details of amino acid interactions of the active site are discussed briefly and correlated with the contour plots.
© 2007 Elsevier Masson SAS. All rights reserved.

*Keywords:* 3D-QSAR; CoMFA; Docking; Triazolopyridine oxazole derivatives

1. Introduction

p38 is a member of Ser/Thr kinases family [1] of the mitogen-activated protein (MAP) kinase super family [2,3]. The four-p38 isoforms, p38-α, p38-β, p38-γ, p38-δ varies based on their substrate specificity. The P38-α (also known as SAPK2α, RK, CSBPs, Mxi2 or Mpk2) [4] and β are responsible for activation of heat shock proteins Hsp 25, 27 and the MAPK activated protein MAPKAP-2 [5]. The actual activation of p38 occurs by dual phosphorylation of conserved Thr and Tyr residues [6] by upstream activators such as MAP kinase kinases (MKKs) upon receiving extra cellular signals [7]. The p38 MAP kinase regulates the release from leukocytes of IL-1 and TNF-α, two cytokines that are associated with the progression of rheumatoid arthritis (RA) [8]. p38 is also implicated in the induction of COX-2, the inducible prostaglandin cyclooxiginase [9]. Inhibitors of the p38-α through their downstream blockage of the production of TNF-α, IL-1β, IL-6, COX-2 and arachidonic acid mobilization have therapeutic potential [10,11]. These inhibitors not only block the synthesis but also the signal cascades induced by these cytokines [12] and prevent activation of caspases and apoptosis of neuronal cells and neuronal progenitor cells [13]. The interest in the development of p38 MAP kinase inhibitors is based on the expectations that p38 inhibiting drugs will treat the underlying cause of chronic inflammatory disease and cease their progression [14]. Although a number of structurally different inhibitors have been reported [15] to inhibit p38 with varying degrees of selectivity, none has reached commercial status [16]. Since, its introduction in 1988, comparative molecular field analysis (CoMFA) [17] has emerged as one of the most

---

* Corresponding author. Tel.: +98 49602498.
*E-mail address:* skmahmood@osmania.ac.in (S.K. Mahmood).

Table 1
Structures of triazolopyridine oxazole derivatives
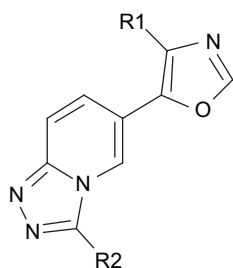
Compound	R1	R2	IC_{50}	Actual pIC_{50}
1	Ph	*i*-Pr	9.6	8.017
2	3-Me—Ph	*i*-Pr	18.3	7.737
3	4-F—Ph	*i*-Pr	5	8.301
4	3-F—Ph	*i*-Pr	37.8	7.422
5	4-F, 5-Me—Ph	*i*-Pr	6.6	8.180
6	2-F, 5-Me—Ph	*i*-Pr	4.3	8.366
7	4-Cl—Ph	*i*-Pr	17.7	7.752
8	3-Cl—Ph	*i*-Pr	13.5	7.868
9	2-Cl—Ph	*i*-Pr	3	8.522
10	2,4-diF Ph	*i*-Pr	4.6	8.337
11	2,5-diF—Ph	*i*-Pr	5.8	8.236
12	2,6-diF—Ph	*i*-Pr	14.6	7.835
13	3,4-diF—Ph	*i*-Pr	22.3	7.651
14	3-Cl, 4-F—Ph	*i*-Pr	12.4	7.906
15	2-F, 4-Cl—Ph	*i*-Pr	2.2	8.657
16	2-F, 5-Cl—Ph	*i*-Pr	5.1	8.292
17	2-Cl, 4-F—Ph	*i*-Pr	2.5	8.602
18	3-F, 4-Cl = Ph	*i*-Pr	43.2	7.362
19	3,4,5-tri F—Ph	*i*-Pr	4.1	8.387
20	2,4,5-tri F—Ph	*i*-Pr	3.2	8.494
21	2,4,6-triF—Ph	*i*-Pr	7.2	8.142
22	2,3,4-triF—Ph	*i*-Pr	11.1	7.954
23	3,4-diCl—Ph	*i*-Pr	26.4	7.578
24	2,4-diCl—Ph	*i*-Pr	8.3	8.080
25	2,3-diCl—Ph	*i*-Pr	14.5	7.838
26	2-F, 4-Cl, 5-F—Ph	*i*-Pr	24.5	7.610
27	2-Cl, 4-F, 5-F—Ph	*i*-Pr	5.6	8.251
28	3-Br, 4-F—Ph	*i*-Pr	8	8.096
29	Ph	Et	54.5	7.263
30	Ph	*c*-Propyl	47.2	7.326
31	Ph	*c*-Bu	16.6	7.779
32	Ph	EtNH	5.4	8.267
33	Ph	EtMeN	9.2	8.036
34	Ph	F_2CH	544	6.264
35	Ph	CF_3CH_2	83.2	7.079
36	4-F—Ph	H	19.5	7.709
37	4-F—Ph	Et	21.6	7.665
38	4-F—Ph	Me_2N	15.3	7.815
39	4-F—Ph	EtNH	7.6	8.119
40	4-F—Ph	EtO	55.5	7.254
41	4-F—Ph	*c*-Bu	17.7	7.752
42	4-F—Ph	*c*-Propyl	10.9	7.962
43	4-F—Ph	*i*-Bu	8.8	8.055
44	4-F—Ph	*i*-PrNH	5.5	8.259
45	4-F—Ph	*n*-Pr-NH	198	6.706
46	4-F—Ph	MeEtN	4.7	8.327
47	4-F—Ph	*i*-PrO	17.9	7.747
48	4-F—Ph	1-Me-*c*-Butyl	14	7.853
49	4-F—Ph	Pyrrolidine	15.4	7.812
50	4-F—Ph	Ph	12.3	7.910
51	4-F—Ph	2-MeOPh	0.4	9.397
52	4-F—Ph	2-EtOPh	0.4	9.397

Table 1 (*continued*)

Compound	R1	R2	IC_{50}	Actual pIC_{50}
53	4-F—Ph	*t*-Bu	3.5	8.455
54	4-F—Ph	Morpholine	11.8	7.928
55	4-F—Ph	$PhCH_2$	19.9	7.701
56	2,4-diF—Ph	*c*-Propyl	3.5	8.455
57	2,4-diF—Ph	1-Me-*c*-Propyl	0.7	9.154
58	2,4-diF—Ph	*c*-Butyl	3.75	8.425
59	2,4-diF—Ph	1-Me-*c*-Butyl	1.1	8.958
60	2,4-diF—Ph	*t*-Bu	1.1	8.958
61	2,4-diF—Ph	2-Propanol-2-yl	25	7.602
62	2,4-diF—Ph	*c*-Propyl	24	7.619
63	2,4-diF—Ph	1-Me-*c*-Propyl	3	8.522
64	2,4-diF—Ph	*c*-Butyl	9.7	8.013
65	2,4-diF—Ph	1-Me-*c*-Butyl	1.5	8.823
66	2,4-diF—Ph	*t*-Bu	8.8	8.055
67	2,4,5-triF—Ph	*c*-Propyl	7.8	8.107
68	2,4,5-triF—Ph	1-Me-*c*-Propyl	2.3	8.638
69	2,4,5-triF—Ph	*c*-Butyl	9.1	8.040
70	2,4,5-triF—Ph	1-me-*c*-Butyl	2.5	8.602
71	2,4,5-triF—Ph	*t*-Bu	1.8	8.744
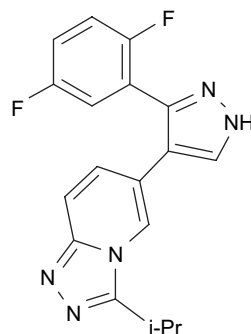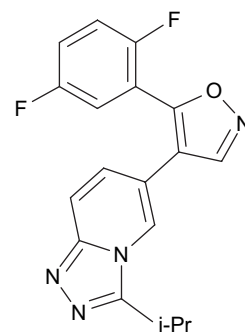
| **72** | | | 2.8 | 8.552 |

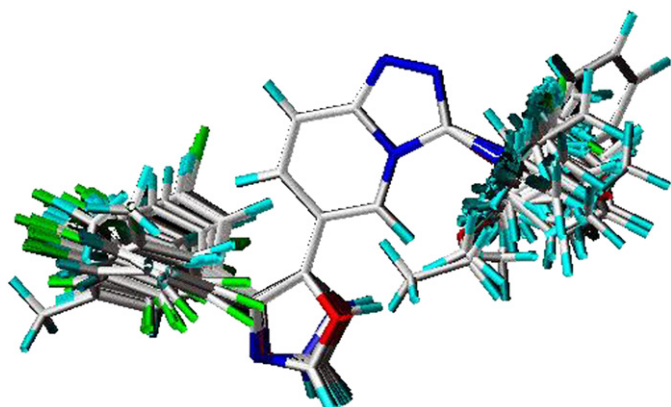| **73** | | | 33.2 | 7.478 |

| **74** | | | 6.2 | 8.207 |
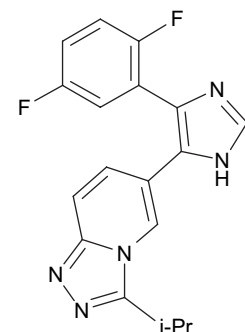
Fig. 1. Alignment of all molecules used for molecular field generation.

powerful tools in ligand based drug design strategies [18]. The CoMFA methodology assumes that a suitable sampling of steric and electrostatic fields around a set of aligned molecules provides all the information necessary for understanding their biological properties [19]. The present study is aimed to gain insight into the steric and electrostatic properties of these compounds, their influence on the activity and to derive predictive 3D-QSAR models to design new class of inhibitors.

2. Computational details

2.1. Molecular modeling

The three-dimensional structures of triazolopyridine oxazole p38 compounds were constructed by using SYBYL programming package version 6.7 [20] on a Silicon Graphics Fuel workstation. Energy minimization was performed using tripos force field [21] and the Gasteiger [22] charge with a distance-dependant dielectric and Powell conjugate gradient algorithm with convergence criterion of 0.05 kcal/mol. Further geometric optimization of these compounds was done using the semi-empirical program MOPAC 6.0 and applying the AM1 Hamiltonian [23]. The MOPAC charges were used for entire calculations.

2.2. Data set

The in vitro biological activity data reported as IC_{50}, for inhibition of p38 alpha kinase by the Triazolopyridine oxazole

Table 2
Summary of CoMFA model result

Component	CoMFA
q^2	0.707
r^2	0.942
r^2_{pred}	0.715
N	5
F value	158.141
SEE	0.157
Steric	0.457
Electrostatic	0.543

q^2, LOO-cross-validated correlation coefficient; r^2, non-cross-validated correlation coefficient; r^2_{pred}, predictive correlation coefficient; n, number of components used in the PLS analysis; SEE, standard error of estimation; F value, F-statistic for the analysis.

Table 3
Actual versus predicted pIC_{50} values for training and test set molecules

Compound	Actual activity	Glide docking score	CoMFA	
			Predicted	Residual
01	8.017	−9.541	7.885	0.132
02	7.737	−9.575	7.868	−0.130
04	7.422	−9.519	7.408	0.015
06	8.366	−9.693	8.490	−0.124
07	7.752	−9.550	8.091	−0.339
08	7.868	−9.164	7.636	0.233
09	8.522	−9.892	8.562	−0.039
10	8.337	−10.313	8.156	0.181
11	8.236	−10.186	8.224	0.012
12	7.835	−9.619	7.674	0.161
13	7.651	−9.013	7.684	−0.032
14	7.906	−9.250	8.088	−0.181
15	8.657	−9.807	8.841	−0.184
16	8.292	−9.980	8.160	0.132
17	8.602	−10.221	8.638	−0.036
18	7.362	−9.849	7.717	−0.353
19	8.387	−10.066	8.066	0.321
20	8.494	−10.0493	8.714	−0.219
21	8.142	−10.514	8.010	0.132
23	7.578	−9.059	7.891	−0.313
24	8.080	−9.835	7.906	0.175
26	7.610	−9.709	7.999	−0.389
28	8.096	−8.938	8.024	0.073
29	7.263	−9.282	7.588	−0.325
30	7.326	−9.176	7.400	−0.074
34	6.264	−8.169	6.843	−0.579
35	7.079	−9.536	6.621	0.458
36	7.709	−8.869	7.410	0.300
38	7.815	−9.993	7.772	0.043
40	7.254	−9.515	7.569	−0.313
41	7.752	−9.191	7.556	0.196
42	7.962	−9.561	7.992	−0.029
43	8.055	−10.011	8.151	−0.095
45	6.706	−8.141	7.616	−0.913
46	8.327	−10.141	7.966	0.362
47	7.747	−9.535	7.779	−0.032
49	7.812	−9.250	8.197	−0.384
50	7.910	−9.119	7.132	0.778
51	9.397	−11.455	8.967	0.431
52	9.397	−11.788	9.476	−0.078
54	7.928	−9.905	7.741	0.187
56	8.455	−10.329	8.541	−0.085
57	9.154	−11.471	8.522	0.633
59	8.958	−10.664	8.423	0.536
60	8.958	−10.658	8.929	0.030
61	7.602	−10.207	8.237	−0.635
62	7.619	−9.593	8.057	−0.437
63	8.522	−10.279	8.120	0.403
64	8.013	−10.337	8.041	−0.028
65	8.823	−10.386	8.188	0.636
68	8.638	−10.581	8.532	0.106
70	8.602	−10.625	8.963	−0.361
71	8.744	−10.714	8.564	0.180
72	8.552	−10.291	8.295	0.258
74	8.207	−9.944	8.564	−0.446
Test Set				
03	8.301	−9.921	7.459	0.842
05	8.180	−9.693	7.534	0.646
22	7.954	−10.39	8.353	−0.399
25	7.838	−9.846	8.290	−0.452
27	8.251	−10.342	8.704	−0.453
31	7.779	−9.781	7.226	0.553

Table 3 (*continued*)

Compound	Actual activity	Glide docking score	CoMFA	
			Predicted	Residual
32	8.267	−9.480	7.533	0.734
33	8.036	−9.715	7.867	0.169
37	7.665	−9.480	7.551	0.114
39	8.119	−9.822	7.352	0.767
44	8.259	−9.891	7.490	0.769
48	7.853	−9.321	8.289	−0.436
53	8.455	−10.275	7.880	0.575
55	7.701	−9.229	7.331	0.370
58	8.425	−10.551	8.876	−0.451
66	8.055	−10.452	8.384	−0.329
67	8.107	−10.344	8.521	−0.414
69	8.040	−10.008	8.559	−0.519
73	7.478	−9.160	8.339	−0.861

compounds were taken from the published work by *McClure* et al. [24] used for the current study (Table 1). The reported IC_{50} values were converted into the corresponding pIC_{50} using the following formula:

$$pIC_{50} = logIC_{50}$$

2.3. Alignment

One of the fundamental assumptions wherein 3D-QSAR studies are based is that a geometric similarity should exist between the structures. In the present study the MOPAC geometry optimized structures were aligned on the template 52, which, is the most active molecule among the given set. All the molecules were aligned by the Align Database command available in SYBYL using maximum substructure. It adjusts the geometry of the molecules such that its steric and electrostatic fields match the fields of the template molecule. The aligned molecules are shown in Fig. 1.

2.4. CoMFA

The steric and electrostatic CoMFA potential fields were calculated at each lattice intersection of a regularly spaced grid of 2.0 Å. The grid box dimensions were determined automatically in such a way that region boundaries were extended beyond 4 Å in each direction from co-ordinates of each molecule. The van dar Waals potentials and Coulombic terms, which represent steric and electrostatic fields, respectively, were calculated using tripos force field. An sp^3 hybridized carbon atom with +1 charge served as probe atom to calculate steric and electrostatic fields.

2.5. Partial least square (PLS) analysis

To quantify the relationship between the structural parameters (CoMFA interaction energies) and the biological activities, the PLS algorithm was used. The CoMFA descriptors were used as independent variables, and pIC_{50} values as dependant variables in partial least square regression analysis.

Cross-validation partial least square method of leave-one-out (LOO) was performed to obtain the optimal number of components used in the subsequent analysis. The minimum sigma (column filtering) was set to 2.0 kcal/mol to improve the signal-to-noise ratio. The optimum number of principle components in the final non-cross-validated QSAR equations was determined to be that leading to the highest correlation coefficient (r^2) and the lowest standard error in the LOO cross-validated predictions. The non-cross-validation was used in the analysis of CoMFA result and the prediction of the model.

2.6. Molecular docking

For the docking of ligands to protein active sites and for estimating the binding affinities of docked compounds, an advanced molecular docking program Glide, version 2.5 [25] was used in this study. During the docking process, initially Glide performs a complete systematic search of the conformational, orientational, and positional space of the docked ligand and eliminating unwanted conformations using scoring and followed by energy optimization. Finally the conformations are further refined via a Monte Carlo sampling of pose conformation. Predicting the binding affinity and rank-ordering ligands in database screens was implemented by modified and expanded version of the ChemScore18 scoring function, Glide Score, for use in. For our studies, X-ray crystal structure of p38 kinase was taken from PDB entry 1ZZL, having resolution of 2.0 Å. Solvent molecules were deleted and bond order for crystal ligand and protein were adjusted and minimized up to 0.30 Å RMSD. Using standard precision (SP) mode of Glide software, docking studies was performed on triazolopyridine oxazole derivatives. The performance of the docking method on p38 inhibitors was evaluated by: re-docking crystal ligand, correlating the docking scores with activity of the triazolopyridine oxazole derivatives as inhibitors of p38 kinase.

3. Results and discussion

The CoMFA method was used for deriving 3D-QSAR model for 55 triazolopyridine oxazole compounds, which are reported as p38 alpha kinase inhibitors. The leave-one-out partial least-squares (PLS) analysis of the obtained model yielded high cross-validated q^2-value of 0.707 (five components) and non-cross-validated correlation coefficient r^2 of 0.942. The steric and electrostatic contributions are 45.7% and 54.3%. The statistical parameters for the developed CoMFA model are presented in Table 2. These correlation coefficients suggest that our model is reliable and accurate. Table 3 lists experimental activities, predicted activities and residual values of the training set and test set by CoMFA model. Fig. 2 shows correlation between the experimental and predicted pIC_{50} values of training and test sets by this CoMFA model.

3.1. 3D contour maps

To visualize the information content of the derived 3D-QSAR model, CoMFA contour maps were generated. The
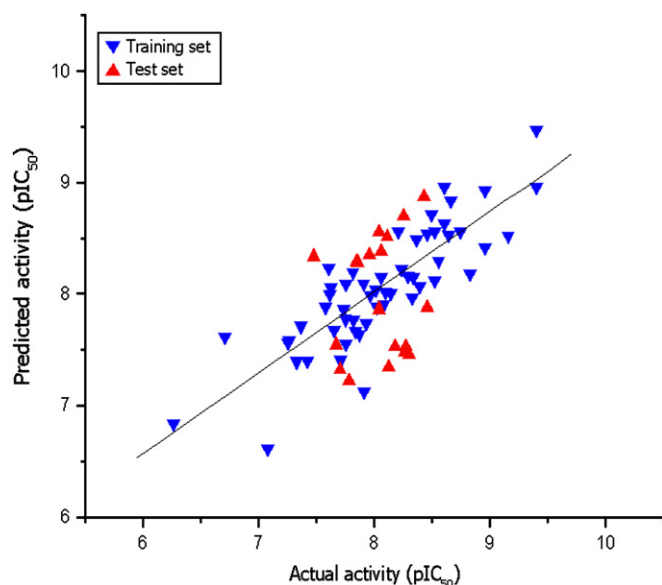
Fig. 2. Plot of actual versus predicted pIC$_{50}$ for CoMFA model.

contour maps have permitted an understanding of the steric and electrostatic requirements for ligand binding. Fig. 3 (a−d) shows the contour maps derived from the CoMFA PLS model. Highly active compound **52** (Fig. 3 a and b) and lowest active compound **34** (Fig. 3 c and d), were embedded in the maps to demonstrate its affinity for the steric and electrostatic regions of inhibitors. The contour plots may help to identify important regions where any change may affect the binding preference. Furthermore, they may be helpful in identifying important features contributing to interactions between the ligand and the active site of a receptor. The steric interactions are represented by green and yellow colored contours whereas electrostatic interactions are displayed as red and blue contours.

3.1.1. Steric contour analysis

In Fig. 3, panels a and c show the steric contours of CoMFA model, which are mainly distributed near the regions of 3-position of the triazolo pyridine and at the 4-position of oxazole ring. Yellow contours indicate regions of steric hindrance to activity, while green region indicate a steric contribution to
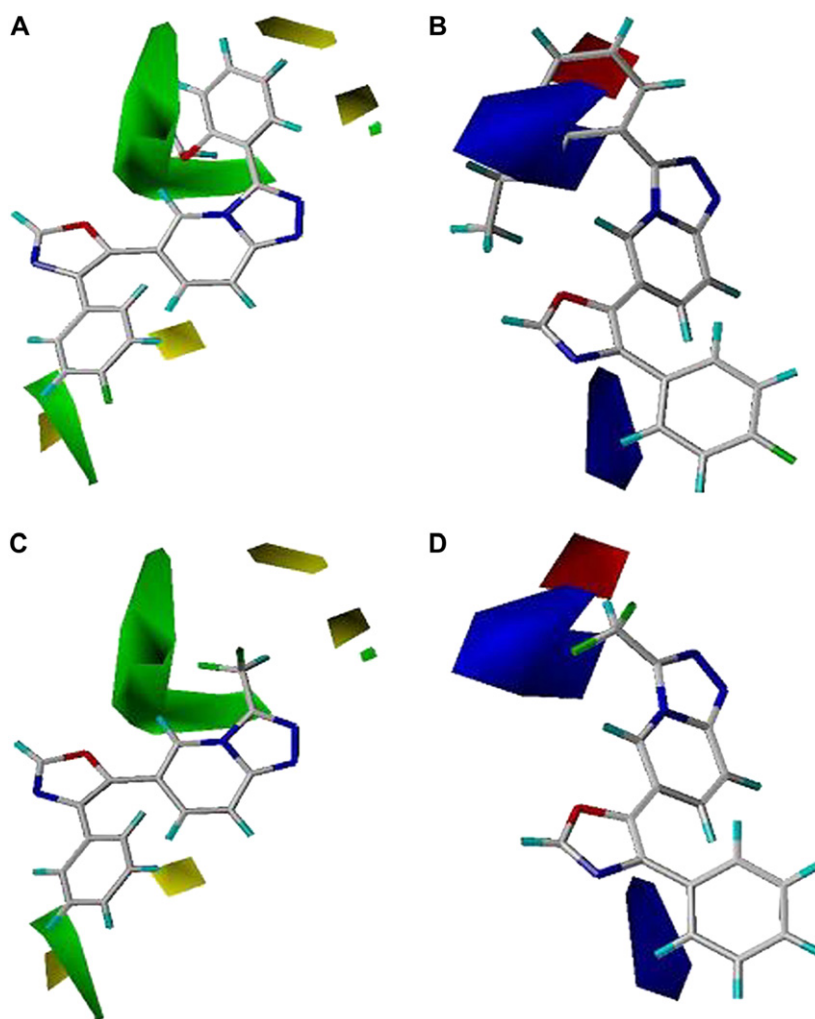
Fig. 3. CoMFA contour maps for p38 alpha inhibitors (A) the steric field distribution and (B) the electrostatic field distribution for high active compound 52 (C) the steric field distribution and (D) the electrostatic field distribution for low active compound 34. Green contour maps for sterically favored areas and sterically disfavored areas are in yellow. Positive potential favored areas are in blue; negative potential favored areas are in red. (For interpretation of the references to color in this figure legend, the reader is referred to the web version of this article.)

potency. As it can be seen in this figure, the highly active compound **52**, orients its substituents, 2-ethoxyphenyl and 4-flurophenyl groups, closer to green areas, while the very low activity of the compound **34** could be due to the orientation of its difloro substituted methyl group to a yellow region. Green map near the *ortho*-position of the phenyl group indicates that bulky substituents may increase the activity. This observation is confirmed by the fact that *ortho*-methoxy phenyl containing ligands (**51**, **52**) always display higher activity compared to the unsubstituted derivatives (**1**, **50**). In phenyl-substituted series, ethyl groups of **35**, **29**, and propyl group of **30** are pointed towards lower yellow contours and have less activity. But the conformational orientation of butyl group and 2-substituted halogens on phenyl ring at 3-position of the triazolo pyridine shows higher activity, as the orientation of these substituents is closer to green contour. This was observed in the compounds **7–9** and **15–18**. The 2,4-difluro phenyl moieties of compounds **56–60** are directed towards the favorable green contour and show higher activity when compared to unsubstituted compounds. In addition, the yellow map near the 5th-position of the phenyl group indicates that bulky substituents there, may decrease the activity. This observation is confirmed by the fact that 2,5-difloro phenyl compounds **61–66** always display lower selectivity compared to the 2,4-difloro phenyl derivatives.

3.1.2. Electrostatic contour analysis

In Fig. 3 (c and d), the electrostatic property maps include **52** and **34** as examples for high and low p38-activity ligands,
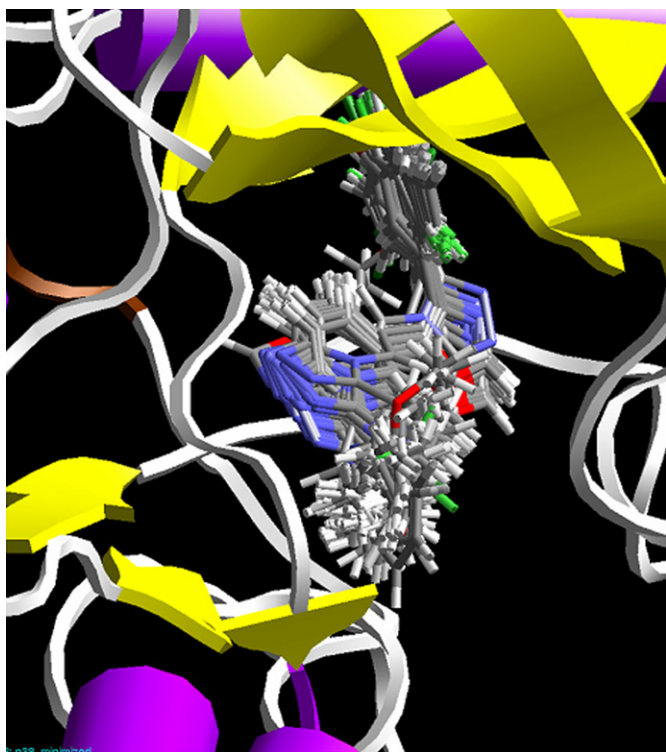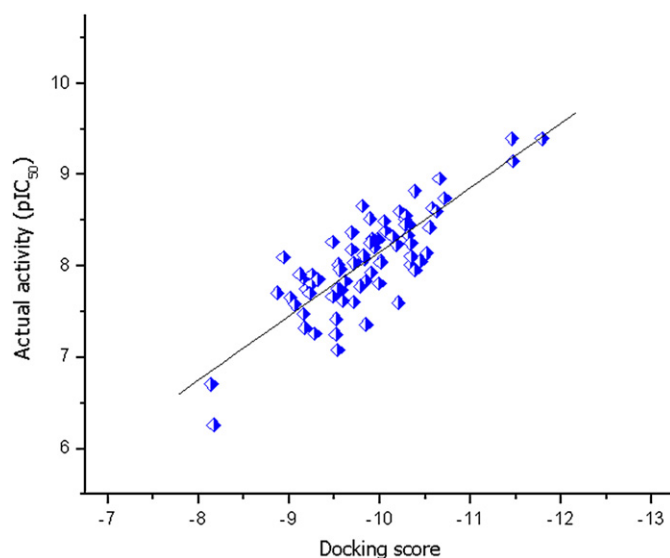

Fig. 5. Plot showing correlation between actual activity and glide docking score.

respectively. The blue regions indicate positive electrostatic charge potential associated with increased activity, while regions of red show negative charge with increased activity. The large blue contour near R2 position of the triazolo pyridine suggests that biological activity can be enhanced by introduction of more electropositive groups at this position. This observation was supported by the compounds **32**, **33**, **38**, **39**, **46**, showing high activities due to the electropositive substituents are closer to this blue contour. A small red contour near R2 position opposite to blue contour indicates electronegative groups are favored at this position. The highest active compounds **51** and **52** orient its substituents near to this contour.

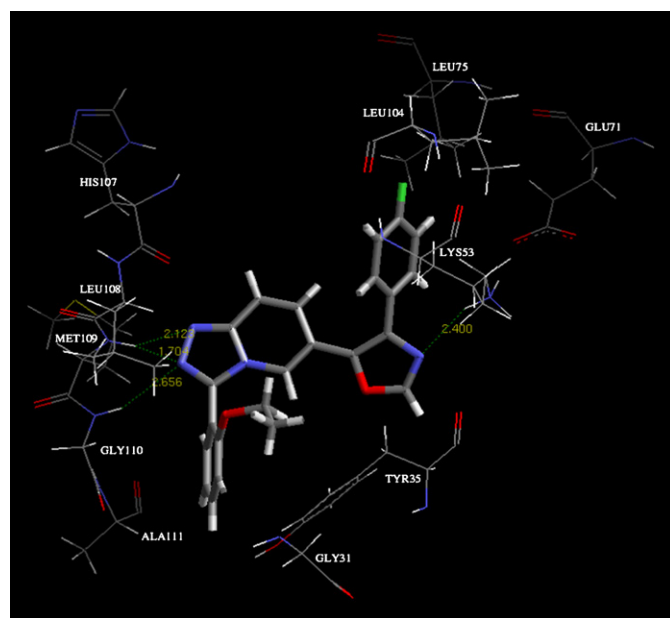Fig. 4. The binding pocket of p38 kinase protein with alignment of docked conformations.

Fig. 6. The position of docked compound **52**, more potent inhibitor in the active site of 1ZZL.
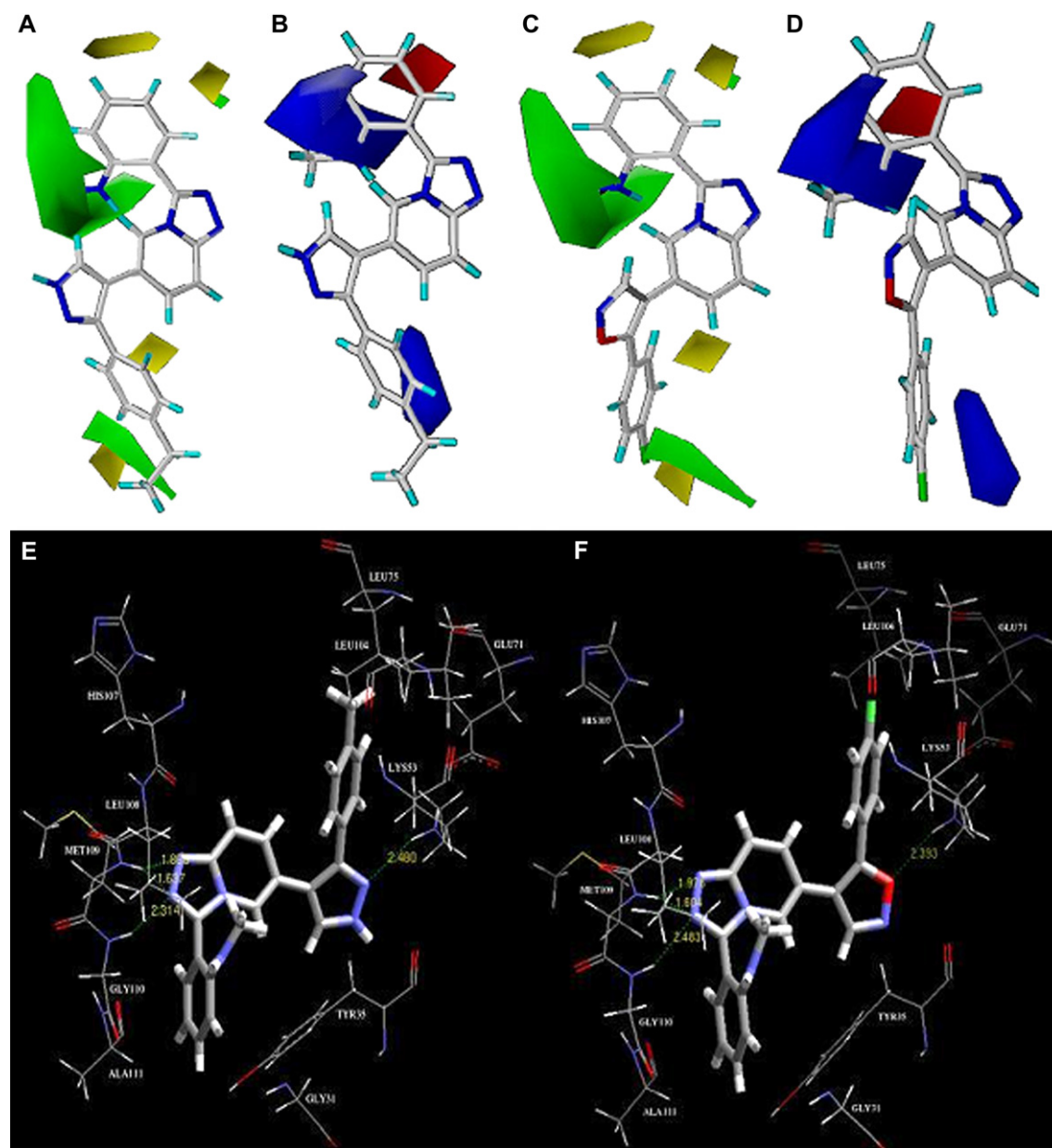
Fig. 7. CoMFA contour maps and binding mode of newly designed molecules for p38 alpha kinase protein (A) the steric field distribution and (B) the electrostatic field distribution for compound A (C) the steric field distribution and (D) the electrostatic field distribution for compound B. (E) Hydrogen bond interactions between p38 kinase protein binding pocket and compound A (F) Hydrogen bond interactions between p38 binding pocket and compound B.

The other blue contours near the R1 aryl ring and bridge five membered hetrocyclic ring support positive charge are favored at this position. The presence of pyrazole ring (**72**) instead of isoxazole (**73**) increases the activity.
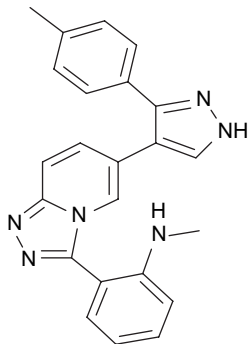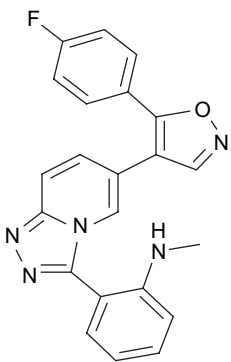
3.2. Docking studies

To investigate the detailed intermolecular interactions between the ligand and the target protein, an automated docking program Glide was used. Three-dimensional structure information on the target protein was taken from the PDB entry 1ZZL; having resolution of 2.0 Å. Processing of the protein included the deletion of the ligand and the solvent molecules as

well as the addition of hydrogen atoms. Standard precision (SP) mode of Glide software was used for the docking studies. All the 74 inhibitors were docked into the active site of p38 as shown in Fig. 4. A correlation was calculated between Glide score and the pIC_{50}s via a linear regression analysis. A good correlation coefficient of 0.827 between experimental pIC_{50} and docking energy (Fig. 5) was obtained. The predicted binding energies of the compounds and the corresponding experimental IC_{50} values are also listed in Table 2.

Fig. 6 shows the docking of highly active molecule **52** in to the active site of p38. As depicted in the figure the *ortho*-substitute phenyl ring at position R2 is placed in the hydrophobic pocket formed by Val38, Val30, Ala50, Ala51 and Leu108.

Table 4
Structures, predicted activities and docking score of newly designed molecules

Compound name	Structure	Predicted activity	Docking score
A		9.548	−11.829
B		9.500	−11.533

A green color contour map of CoMFA model is appeared at this position suggesting for bulky substituents at this position. Another hydrophobic pocket is formed by the amino acids Lys53, Leu74, Glu71, and Leu104. *para*-Substituted phenyl ring positioned at R1 of the ligand, is positioned into this pocket. It was suggested by green color contour at this position. Two yellow contours of CoMFA model appeared in R2 is occupied by the amino acids Tyr35, Gly 110, Ala111, Leu156, Asn115, of docking model, suggesting that no space for substitutions. A high level of selectivity for specific kinase target, the inhibitors should have interactions with backbone amino acids present in the hinge region of protein [26]. The molecule is also forming three strong H-bonds with Hinge region amino acids. Two-electron rich nitrogen triazolopyridine ring is forming three hydrogen bonds with main chain NH of amino acids Gly110 and Met109 present in the hinge region. Another hydrogen bond is formed between electron rich nitrogen of oxazole ring and side chain NH of Lys53.

Designing of potent analogs: Based on the results of CoMFA and docking studies, we have designed two compounds by substituting suitable groups at R1 and R2 position. We have followed same procedure of minimization for these molecules, which were implemented for 74 known actives. All these molecules were aligned and activity was predicted using CoMFA model (Fig. 7 panel a– d). Interestingly these molecules are showing higher activity as the substituents on

these molecules are well mapping to the contours of the CoMFA model. These two molecules were also docked into the active site of p38 kinase and they are showing high docking score (Fig. 7 panel e and f). The Table 4 shows the structure, CoMFA predicted activity and Glide docking score.

4. Conclusion

3D QSAR analyses have been performed on 74 triazolopyridine oxazole derivatives as inhibitors for p38 alpha kinase inhibitors using CoMFA. A satisfactory CoMFA model was obtained to predict the activities of test set structures. The good correlation of 0.715 between experimental and predicted pIC_{50} values for the test compounds further proved the predicted power of the constructed QSAR model. Binding conformations of 74 triazolopyridine oxazole derivatives were predicted by molecular docking program, Glide. There is good correlation between Glide score and activity of 0.827. The quality of QSAR model was also shown with the most important residues of the active site of p38 MAP kinase. Docking and CoMFA results provide useful information in understanding the structural features of the target and chemical features of the ligands. This was extended to the successful designing of highly active analogs of triazolopyridine oxazole derivatives against p38 kinase.

References

[1] P. Sandra, J.P. Maria, M.C. Pedro, S.M. Victoria, R.G. Ana, C. Piero, M. Federico Jr., M. Cristina, Curr. Biol. 16 (2006) 2042–2047.
[2] J.C. Lee, J.T. Laydon, P.C. McDonnell, T.F. Gallagher, S. Kumar, D. Green, D. McNulty, M.J. Blumenthal, J.R. Heys, S.W. Landvatter, J.E. Stricker, M.M. McLaughlin, J.R. Siemens, S.M. Fisher, G.P. Livi, J.R. White, J.L. Adams, P.R. Young, Nature 372 (1994) 739.
[3] J. Hans, J.-D. Lee, L. Bibbs, R.J. Ulevitch, Science 265 (1994) 808.
[4] B.L. Rachel, H. Steven, W. Rebecca, F.P. Hugh, J.M. Christopher, Curr. Biol. 8 (1998) 1049–1057.
[5] J.C. Kyra, B.S. Kenneth, J. Exp. Biol. 206 (2003) 107.
[6] J.B. Alastair, K. Stefan, Trends Pharmacol, Sci. 27 (2006) 525–530.
[7] A.M. Badger, J. Bradbeer, B. Votta, J.C. Lee, J.L. Adams, D.E. Griswals, J. Pharm. Exp. Ther 279 (1996) 1453.
[8] A.H. Julianne, K. Florida, D.R. Rowena, J.S. Peter, Ida Ita, X.M. Sherrie, V.P. James, E.C.A. Cornelis Hop, K. Sanjeev, W. Zhen, J.O. Stephen, A.O. Edward, P. Gene, E.T. James, W. Andrew, M.Z. Dennis, B.D. James, Bioorg. Med. Chem. Lett. 13 (2003) 467.
[9] J.C. Lee, M.J. Blumenthal, J.T. Laydon, K.B. Tan, D.L. DeWitt, W.W. Lin, B.C. Chen, J. Pharmacol. 126 (1999) 1419.
[10] A.D. Mark, A.L. Michael, F.M.C. Kim, T.B. John, J.C. Thomas, R.C. Santo, C. Csilla, J.D. Alan, C.E. Nancy, A.G. Christopher, K.J. Crystal, M.L. Jeff, H.M. William, M.P. Kevin, A.S. Ingrid, S. Linne, J.S. Francis, H.Y. Chul, Bioorg. Med. Chem. Lett. 14 (2004) 919–923.
[11] J.L. Adams, A.M. Badger, S. Kumar, J.C. Lee, Prog. Med. Chem. 38 (2001) 1.

[12] S. Kumar, P.C. McDonnell, R.J. Gum, A.T. Hand, J.C. Lee, P.R. Young, Biochem. Biophys. Res. Commun. 235 (1997) 533.

[13] J. Harada, M. Sugimoto, Jpn. J. Pharmacol. 79 (1999) 369–378.

[14] R. Laszlo, E.D. Franco, B. Thomas, F. Roland, G. Hermann, H. Pete, M. Ute, W. Romain, G.Z. Alfred, Bioorg. Med. Chem. Lett. 12 (2002) 2109.

[15] (a) C. Dominguez, D.A. Powers, N. Tamayo, Curr. Opin. Drug. Disc. 8 (2005) 421;
(b) D.M. Goldstein, T. Gabriel, Curr. Top. Med. Chem. 10 (2005) 1017.

[16] (a) J. Hynes, K. Leftheris, Curr. Top. Med. Chem. 10 (2005) 967;
(b) F.G. Salituro, R.A. Germann, K.P. Wilson, G.W. Bemis, T. Fox, M.S.-S. Su, Curr. Med. Chem. 6 (1999) 807.

[17] R.D. Cramer III, D.E. Patterson, J.D. Bunce, J. Am. Chem. Soc. 110 (1998) 5959–5967.

[18] G.R. Desiraju, B. Gopalakrishnan, R.K. Jetti, A. Nagaraju, J.D. Raveendra, A. Sharma, M.E. Sobhia, R. Thilagavathi, J. Med. Chem. 45 (2002) 4847–4857.

[19] S.K. Singh, N. Dessalew, P.V. Bharatam, Eur. J. Med. Chem. 41 (2006) 1310–1319.

[20] SYBYL, version 6.8, Tripos Associates, St. Louis, MO, 2000.

[21] M. Clark, R.D. Cramer III, N. Van Opdenbosch, J. Comput. Chem. 10 (1989) 982–1012.

[22] J. Gasteiger, M. Marsilli, Tetrahedron 36 (1980) 3219.

[23] J.J.J. Stewart, Comput. Aided Mol. Des. 4 (1990) 1.

[24] K.F. McClure, M.A. Letavic, A.S. Kalgutkar, C.A. Gabel, L. Audoly, J.T. Barberia, J.F. Braganza, D. Carter, T.J. Carty, S.R. Cortina, M.A. Dombroski, K.M. Donahue, N.C. Elliot, C.P. Gibbons, C.K. Jordan, A.V. Kuperman, J.M. Lebasi, R.E. LaLiberte, J.M. McCoy, B.M. Naiman, K.L. Nelson, H.T. Nguyen, K.M. Peese, F.J. Sweeney, T.J. Taylor, C.E. Trebino, Y.A. Abramov, E.R. Laird, W.A. Volberg, J. Zhou, J. Bach, F. Lombardo, Bioorg. Med. Chem. Lett. 16 (2006) 4339–4344.

[25] Glide, www.schrodinger.com, NY.

[26] E. Perola, Proteins 64 (2006) 422–435.